



OPEN

Significance of thermal radiation and bioconvection for Williamson nanofluid transportation owing to cone rotation

Sohaib Abdal^{1,2}, Imran Siddique^{3✉}, Sayed M. Eldin⁴, Muhammad Bilal¹ & Sajjad Hussain⁵

Numerical investigation for enhancement in thermal distribution of unsteady dynamics of Williamson nanofluids and ordinary nanofluids flow across extending surface of a rotating cone is represented in this communication. Bio-convection of gyrotactic micro-organisms and thermal radiative fluxes with magnetic fields are significant physical aspects of the study. The velocity slip conditions are considered along x and y directions. The leading formulation is transmuted into ordinary differential form via similarity functions. Five coupled equations with non-linear terms are resolved numerically through the utilization of Matlab code for the Runge–Kutta procedure. The parameters of buoyancy ratio and bio-convection Rayleigh number decrease the x-direction velocity. The slip parameter being proportional to viscosity reduces the speed of flow and hence rise in temperature. Also, the temperature rises with the rising values of magnetic field strength, radiative heat transportation, Brownian motion and thermophoresis.

Latin symbols

u, v, w	Velocity components (m/s)
x, y, z	Cartesian coordinates (m)
B_o	Magnetic field strength (T)
C	Concentration of nanoparticles
T	Temperature of nanoparticles (K)
n	Micro-organisms distribution
g	Gravity (m/s^2)
k^*	Mean absorption co-efficient (1/m)
k	Thermal conductivity (W/m K)
$\rho_p C_p$	Effective heat capacity (J/K)
D_B	Brownian diffusion coefficient (m^2/s)
D_T	Thermophoresis diffusion coefficient (m^2/s)
D_m	Diffusivity of microorganisms (m^2/s)
T_∞	Ambient temperature (K)
C_∞	Ambient concentration of nanoparticles
n_∞	Ambient micro-organisms distribution
c_b	Chemotaxis constant (m)
W_c	Speed of gyrotactic cell (m/s)
q_w	Heat transfer rate (W/m^2)
M	Magnetic parameter
Nr	Buoyancy ratio parameter
Rb	Rayleigh number

¹Department of Mathematics, Khwaja Fareed University of Engineering and Information Technology, Rahim Yar Khan 64200, Pakistan. ²School of Mathematics, Northwest University, No. 229 North Taibai Avenue, Xi'an 7100069, China. ³Department of Mathematics, University of Management and Technology, Lahore 54770, Pakistan. ⁴Center of Research, Faculty of Engineering, Future University in Egypt, New Cairo 11835, Egypt. ⁵School of Aerospace and Mechanical Engineering, Nanyang Technological University, Singapore, Singapore. ✉email: imransmsrazi@gmail.com

Rd	Radiation parameter
Pr	Prandtl number
Nb	Brownian motion parameter
Nt	Thermophoresis parameter
Lb	Bio-convection Lewis number
Pe	Peclet number

Greek symbols

α^*	Semi vertical angle
β	Williamson fluid parameter
β_c	Concentration coefficient
β_t	Thermal coefficient
ν_0	Kinematic viscosity (m^2/s)
σ	Electrical conductivity (S/m)
σ^*	Stefan–Boltzmann constant ($\text{W m}^{-2} \text{K}^{-4}$)
ρ	Density (kg/m^3)
η	Similarity variable
θ	Similarity temperature
ϕ	Similarity concentration of nanoparticles
χ	Similarity density of micro-organisms
δ	Microorganisms concentration difference

Nanofluids play vital role in the current era because of its enormous diversity and complexity. They are being used in various applications such as in the petroleum industry, medical applications, food processing and many more. Firstly, the concept of nanofluid was given by Choi and Eastman¹. They discussed the role of thermal conductivity of nano particles in base fluids. Abbas et al.² scrutinized the 2nd-Grade nanofluid flow for unsteady case having thermal radiation and mixed convection. Wang et al.³ investigated the effects of nanoparticle accumulation and radiation on the flow of nanofluid. Gowda et al.⁴ computationally studied the effects of Stefan blowing on 2nd grade fluid. Kumar et al.⁵ investigated the influence of activation energy over Darcy-Forchheimer flow of Casson fluid in a porous media. Gowda et al.⁶ studied sedimentation of thermophoretic particles in unsteady hybrid nanofluid. Jyothi et al.⁷ elaborated the effects of thermal radiation on casson fluid for non linear case using Buongiorno's nanofluid model. Li et al.⁸ analysed the hybrid nanofluid in nonlinear mixed convective flow along with entropy. Yusuf et al.⁹ investigated MHD Williamson nanofluid along with gyrotactic organisms. Prasannakumara¹⁰ numerically studied transport of heat in Maxwell nanofluid flow. Benos et al.¹¹ examined the MHD convection of CNT-Water nanofluid using Hamilton-Crosser model. Sarris et al.¹² studied the large-eddy simulations (LES) of turbulent and transitional channel flows of a conductive fluid under the effect of a uniform magnetic field. Sarris et al.¹³ presented a study of the flow field and residence times in the anode flow bed of a pilot direct ethanol fuel cell (DEFC) using 3-D numerical flow modelling. Karvelas et al.¹⁴ studied the micromixing efficiency of particles in heavy metal removal processes. Gowda et al.^{15–19} studied the nanofluid flow for different geometries.

An English mathematician Williamson developed the Williamson fluid model²⁰ in 1929 and numerous researchers considered it. Williamson fluid is a non-Newtonian fluid model which has a shear thinning property. Srinivas et al.²¹ explored the importance of lubrication of surfaces and convective boundary conditions in the flow of non-Newtonian Williamson fluid. Abdal et al.²² investigated MHD Williamson Maxwell nanofluid over a sheet. Qayyum et al.²³ studied the Williamson nanofluid flow for radiation and velocity slip. Waqas et al.²⁴ studied the Fick's and Fourier's concept for heat production in nonlinear convective Williamson nanofluid flow. Chu et al.²⁵ studied about the thermal energy of hybrid nanoparticles by engaging chemical reaction and activation energy. Chu et al.²⁶ elaborated the properties of thermal radiation, heat generation and the effect of convective boundary conditions. Similar work was done by many researchers^{22,27–29}

Bio-convection can be termed as hydrodynamic instability and designs in suspensions of biased swaying microorganisms. Bioconvection has several uses in the field of natural systems and biotechnology. Various researchers uses bio-convection of living microorganisms to explore the behavior of fluid. Ramesh et al.³⁰ investigated Maxwell nanofluid having gyrotactic organisms along with nonlinear thermal radiation. Song et al.³¹ discussed the micropolar nanofluid for nonlinear thermal radiation having gyrotactic organisms flow and moreover Applications of modified Darcy law. Farooq et al.³² studied the bioconvection in Carreau nanofluid flow having numerous thermal consequences. Song et al.³³ explored the gyrotactic analysis of Sutterby nanofluid having many thermal features. Chu et al.³⁴ Collective effect of Cattaneo-Christov double diffusion and radiative heat flux on gyrotactic organisms flow of Maxwell liquid. Yahya et al.²⁹ scrutinized the thermal characteristics of Williamson Sutterby nanofluid through sponge medium.

This survey of past studies convinced that bioconvection of microorganisms immersed in Williamson nanofluid flow across a rotating cone is rarely discussed. The nanofluid flow across the slip surface of the cone in the presence of magnetic field and thermal radiation adds to the physical aspects of this work. There seems a gap to explore:

(1) The impact of nano particle distribution on flow across a rotating cone.

(2) How does the bioconvection, magnetic field and thermal radiation affect the Williamson nanofluid slip transportation?

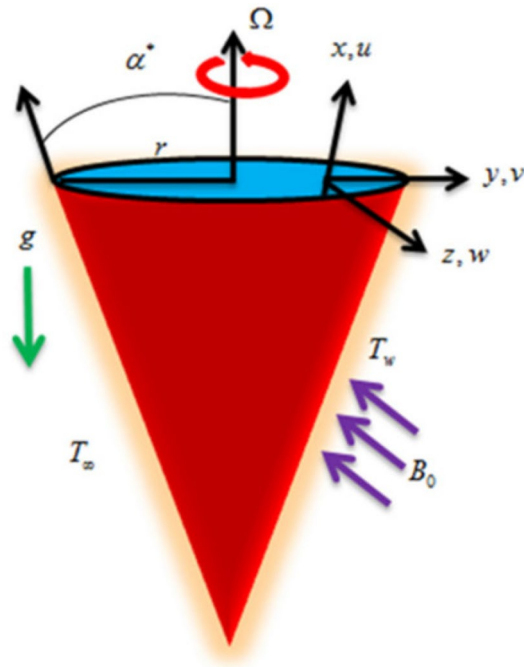


Figure 1. Flow chart.

The motivation of this work pertains to enhancement of thermal distribution to increase thermal conductivity of base fluid with inclusion of nano-entities. The apprehension of the possible settling of nano-material is dismantled through density gradients of microorganisms. Thus bioconvection is considered along with nanofluid transportation across the cone. These physical aspects with heat and mass flow across cone geometry are practicable in rotational dynamical systems. The results can find applications in the efficient working of heat exchangers, cooling of microelectronics and transfer engines.

Flow assumption and mathematical formulation

Considered the unsteady and incompressible Williamson nanofluid with thermal radiation and microorganisms flowing past a rotating cone. Assuming cone rotation velocity as a function of time causes unsteadiness in the flow field. The mass, temperature and microorganisms' difference in the flow field induce the existence of buoyancy forces. Velocity components u , v and w are along x , y and z directions. Cone rotation is represented by Ω (see Fig. 1). The flow velocity slips are considered in x and y directions. A magnetic field of strength B_0 acts perpendicular to the x -axis. The cone half angle is α^* . The self motile micro-organisms are dilutely mixed with base fluid. The motion of micro-organisms does not depend on the transport of nano particles and vice versa. The temperature, nano particle concentration and micro-organisms have constant wall conditions. Hall effect is taken in to consideration. The formulation of the leading equations is presented as^{35–40}.

$$\frac{\partial(xu)}{\partial x} + \frac{\partial(xw)}{\partial z} = 0, \tag{1}$$

$$\begin{aligned} \frac{\partial u}{\partial t} + u \frac{\partial u}{\partial x} - \frac{v^2}{x} + w \frac{\partial u}{\partial z} &= v_0 \left(\frac{\partial^2 u}{\partial z^2} + \sqrt{2}\Gamma \left(\frac{\partial u}{\partial z} \right) \frac{\partial^2 u}{\partial z^2} \right) - \frac{\sigma B_0^2 (u + mv)}{\rho(1 + m^2)} \\ &+ \frac{1}{\rho} \left(\beta_M (1 - C_\infty) \rho g (T - T_\infty) - (\rho_p - \rho) g (C - C_\infty) - (n - n_\infty) g \gamma (\rho_m - \rho) \right), \end{aligned} \tag{2}$$

$$\frac{\partial v}{\partial t} + u \frac{\partial v}{\partial x} + \frac{uv}{x} + w \frac{\partial v}{\partial z} = v_0 \left(\frac{\partial^2 v}{\partial z^2} + \sqrt{2}\Gamma \left(\frac{\partial v}{\partial z} \right) \frac{\partial^2 v}{\partial z^2} \right) - \frac{\sigma B_0^2 (mv - v)}{\rho(1 + m^2)}, \tag{3}$$

$$\frac{\partial T}{\partial t} + u \frac{\partial T}{\partial x} + w \frac{\partial T}{\partial z} = \frac{k}{\rho c_p} \left(\left(\frac{\partial u}{\partial z} \right)^2 + \left(\frac{\partial v}{\partial z} \right)^2 \right) + \frac{16T_\infty^3 \sigma^*}{3k^* \kappa} \frac{\partial}{\partial z} \frac{\partial T}{\partial z} + \frac{\sigma B_0^2 (u^2 + v^2)}{\rho c_p} + \tau D_B \frac{\partial C}{\partial z} \frac{\partial T}{\partial z} + \tau \frac{D_T}{T_\infty} \left(\frac{\partial T}{\partial z} \right)^2, \tag{4}$$

$$\frac{\partial C}{\partial t} + u \frac{\partial C}{\partial x} + w \frac{\partial C}{\partial z} = D_B \frac{\partial}{\partial z} \frac{\partial C}{\partial z} + \frac{D_T}{T_\infty} \frac{\partial}{\partial z} \frac{\partial T}{\partial z}, \tag{5}$$

$$\frac{\partial n}{\partial t} + u \frac{\partial n}{\partial x} + w \frac{\partial n}{\partial z} + \frac{c_b W_c}{C_w - C_\infty} \left(\frac{\partial}{\partial z} \left(n \frac{\partial C}{\partial z} \right) \right) = D_m \frac{\partial}{\partial z} \frac{\partial n}{\partial z}. \tag{6}$$

with suitable boundary conditions

$$\left. \begin{aligned} u = N_0 \mu \frac{\partial u}{\partial z}, v = \frac{\Omega x \sin \alpha^*}{1 - qt^*} + N_0 \mu \frac{\partial v}{\partial z}, w = 0, T = T_w, C = C_w, n = n_w, \text{ at } \eta = 0, \\ u = 0, v = 0, T = T_\infty, C = C_\infty, n = n_\infty, \text{ as } \eta \rightarrow \infty. \end{aligned} \right\} \tag{7}$$

Using similarity transformations

$$\left. \begin{aligned} u = \frac{-\Omega x \sin \alpha^*}{2(1 - qt^*)} f'(\eta), v = \frac{\Omega x \sin \alpha^*}{(1 - qt^*)} g(\eta), w = \sqrt{\frac{\nu_0 \Omega \sin \alpha^*}{(1 - qt^*)}} f'(\eta), \\ \theta(\eta) = \frac{T - T_\infty}{T_w - T_\infty}, T_w - T_\infty = \frac{x(T_0 - T_\infty)}{L(1 - qt^*)^2}, \phi(\eta) = \frac{C - C_\infty}{C_w - C_\infty}, C_w - C_\infty = \frac{x(C_0 - C_\infty)}{L(1 - qt^*)^2}, \\ \chi(\eta) = \frac{n - n_\infty}{n_w - n_\infty}, n_w - n_\infty = \frac{x(n_0 - n_\infty)}{L(1 - qt^*)^2}, t^* = (\Omega \sin \alpha^*) t, \eta = \sqrt{\frac{\Omega \sin \alpha^*}{\nu_0(1 - qt^*)}} z. \end{aligned} \right\} \tag{8}$$

The transformed ordinary differential equations are:

$$f'''(1 - \beta f'') + \frac{f'^2}{2} - 2g^2 - ff'' - S(f' + \frac{\eta}{2} f'') - 2\lambda(\theta - Nr\phi - Rb\chi) - \frac{M}{1 + m^2}(f' - 2mg) = 0, \tag{9}$$

$$g''(1 + \beta g') + gf' - fg' - S(g + \frac{\eta}{2} g') - \frac{M}{1 + m^2}(\frac{mf'}{2} + g) = 0, \tag{10}$$

$$(1 + Rd)\theta'' - Pr \left(S(2\theta + \frac{\eta}{2} \theta') - \frac{f'\theta}{2} + f\theta' \right) + Br(\frac{f'^2}{4} + g'^2) + MBr(\frac{f'^2}{4} + g^2) + Nb\theta'\phi' + Nt\theta'^2 = 0, \tag{11}$$

$$\phi'' - Sc \left(S(2\phi + \frac{\eta}{2} \phi') - \frac{f'\phi}{2} + f\phi' \right) + (\frac{Nt}{Nb})\theta'' = 0, \tag{12}$$

$$\chi'' - Lb \left(S(2\chi + \frac{\eta}{2} \chi') - \frac{f'\chi}{2} + f\chi' \right) + Pe[\phi''(\chi + \delta) + \chi'\phi'] = 0. \tag{13}$$

with transformed boundary conditions are:

$$\left. \begin{aligned} f(0) = 0, f'(0) = \Delta_u f''(0), g(0) = 1 + \Delta_u g'(0), \theta(0) = 1, \phi(0) = 1, \chi(0) = 1, \text{ at } \eta = 0, \\ f'(\infty) \rightarrow 0, g(\infty) \rightarrow 0, \theta(\infty) \rightarrow 0, \phi(\infty) \rightarrow 0, \chi(\infty) \rightarrow 0, \text{ as } \eta \rightarrow \infty. \end{aligned} \right\} \tag{14}$$

Where the non-dimensional parameters are $\beta = \Gamma x \sqrt{\frac{1}{2\nu_0} \left(\frac{\Omega \sin \alpha^*}{1 - qt^*} \right)^3}$ Williamson fluid parameter, $M = \frac{\sigma B_0^2(1 - qt^*)}{\rho \Omega \sin \alpha^*}$ is magnetic parameter, $Nr = \frac{(\rho_p - \rho)(C - C_\infty)}{\beta_M(1 - C_\infty)\rho(T - T_\infty)}$ represents buoyancy ratio parameter, $Rb = \frac{\gamma(\rho_m - \rho)(n - n_\infty)}{\beta_M(1 - C_\infty)\rho(T - T_\infty)}$ is Rayleigh number, $\lambda = \frac{Gr}{Re^2}$ is mixed convection parameter, $Gr = \frac{g\beta_1 \cos \alpha^*(T - T_\infty)L^3}{\nu_0^2}$ is Grashof number, $Re = \frac{L^2 \Omega \sin \alpha^*}{\nu_0}$ is Reynolds number, $Sc = \frac{\nu}{D_B}$ represents Schmidt number, $Pr = \frac{k}{\alpha}$ is the Prandtl number, radiation parameter is $Rd = \frac{16T_\infty^3 \sigma^*}{3k^*}$, Peclet number is $Pe = \frac{c_b W_c}{\nu_0}$, bioconvection Lewis number is $Lb = \frac{\nu}{D_m}$, Brownian motion parameter is $Nb = \frac{\tau D_B (C - C_\infty)}{(1 - qt^*)^2 L}$ and thermophoresis parameter is $Nt = \frac{\tau D_T (T - T_\infty) \Omega \sin \alpha^*}{T_\infty (1 - qt^*)^2 L \nu_0}$.

Physical quantities

Skin friction coefficient. The coefficient of surface drag is represented by:

$$Cf_x = \frac{2\tau_{xz}}{\rho \left(\frac{\Omega \sin \alpha^*}{1 - qt^*} \right)^2}$$

where, τ_{xz} is a shear stress detector and is defined as:

$$\tau_{xz} = \mu(1 + \beta) \left(1 + \frac{\Gamma}{2} \frac{\partial u}{\partial z} \right) \frac{\partial u}{\partial z} \text{ at } z = 0$$

Applying Eq. (8), the dimensionless formulation of the preceding equation is:

$$Cf_x(Re_x)^{\frac{1}{2}} = -(f''(0) + \beta(f''(0))^2)$$

also

$$Cf_y = \frac{2\tau_{yz}}{\rho \left(\frac{\Omega \sin \alpha^*}{1 - q t^*} \right)^2}$$

where, τ_{yz} is a shear stress detector and is defined as:

$$\tau_{yz} = \mu(1 + \beta) \left(1 + \frac{\Gamma}{2} \frac{\partial v}{\partial z} \right) \frac{\partial v}{\partial z} \quad \text{at } z = 0$$

Applying Eq. (8) the dimensionless formulation of the preceding equation is:

$$Cf_y(Re_x)^{\frac{1}{2}} = -(g'(0) + \beta(g'(0))^2)$$

Local Nusselt number. The mathematical solution for the heat transfer efficiency relationship is as described in the following:

$$Nu_x = \frac{xq_w}{k(T_w - T_\infty)}$$

The external heat transfer is:

$$q_w = -\frac{\partial T}{\partial z} - \frac{16T_\infty^3 \sigma^*}{3k^*} \frac{\partial T}{\partial z} \quad \text{at } z = 0$$

Using Eq. (8), the preceding solution is reduced as follows:

$$Nu_x(Re_x)^{-1/2} = -(1 - Rd)\theta'(0)$$

Sherwood number. It is defined as:

$$Sh_x = \frac{xq_m}{k(C_w - C_\infty)}$$

where q_m stands for surface mass flow and is denoted as:

$$q_m = -D_B \frac{\partial C}{\partial z} \quad \text{at } z = 0$$

Using Eq. (8), the above equation's non-dimensional version is:

$$Sh_x(Re_x)^{-1/2} = -\phi'(0)$$

Density of micro-organisms. It is defined as:

$$Nn_x = \frac{xq_n}{k(n - n_\infty)} \quad (15)$$

where q_n identifies the flux of motile microorganisms and is delineated as:

$$q_n = -D_n(C) \frac{\partial n}{\partial z} \quad \text{at } z = 0 \quad (16)$$

Using Eq. (8), the non-dimensional form of equation is:

$$Nn_x(Re_x)^{-\frac{1}{2}} = -\chi'(0)$$

Numerical procedure

This section describes numerical procedure for the leading ordinary differential Eqs. (9)–(13) with boundary conditions (14). Such type of boundary value problems is difficult to solve analytically. Although various numerical approaches are being used for this purpose, yet Range–Kutta (R–K) fourth order method is frequently utilized (see^{41–45}). We also hired R–K method for the solution of the problem. To carry out this strategy, the governing Eqs. (9)–(14) are converted into a first-order differential form as shown below:

<i>Pr</i>	λ	Chamka et al. ³⁵	Deebani et al. ³⁶	Present Results
0.7	0.0	1.0255	1.022543	1.022535
0.7	1.0	2.2015	2.201024	2.201036
0.7	10.0	8.5041	8.504256	8.504233
10.0	0.0	1.0256	1.025543	1.025561
10.0	1.0	1.5636	1.563001	1.563422
10.0	10.0	2.0201	2.082000	2.024200

Table 1. The comparative outputs with respect to *x*.

<i>Pr</i>	λ	Chamka et al. ³⁵	Deebani et al. ³⁶	Present Results
0.7	0.0	0.6158	0.615430	0.615545
0.7	1.0	0.8494	0.849312	0.849462
0.7	10.0	1.3995	1.399221	1.399365
10.0	0.0	0.6158	0.615831	0.615442
10.0	1.0	0.6837	0.683534	0.683664
10.0	10.0	0.9840	0.984555	0.986325

Table 2. The comparative outputs with respect to *y*.

$$\begin{aligned}
 y'_1 &= y_2 \\
 y'_2 &= y_3 \\
 y'_3 &= \frac{-1}{1-\beta f''} \left[\frac{1}{2} f'^2 - f'' - 2g^2 - S \left(f' + \frac{1}{2} \eta f'' \right) - \frac{M}{1+m^2} (f' - 2mg) - 2\lambda(\theta - Nr\phi - Rb\chi) \right] \\
 y'_4 &= y_5 \\
 y'_5 &= \frac{-1}{1-\beta g'} \left[-fg' + f'g - S \left(g + \frac{1}{2} \eta g' \right) - \frac{M}{1+m^2} \left(g + \frac{mf'}{2} \right) \right] \\
 y'_6 &= y_7 \\
 y'_7 &= \frac{-1}{1+Rd} \left(-Pr \left[f\theta' - \frac{1}{2} f'\theta + S(2\theta + \frac{1}{2} \eta \theta') \right] + PrEc \left(\frac{f'^2}{4} + g'^2 \right) + MPPrEc \left(\frac{f'^2}{4} 6 + g^2 \right) + Nb\theta'\phi' + Nt\theta'^2 \right) \\
 y'_8 &= y_9 \\
 y'_9 &= Sc \left[f\phi' - \frac{1}{2} f'\phi + S \left(2\phi + \frac{1}{2} \eta \phi' \right) \right] - \left(\frac{Nt}{Nb} \right) \theta'' \\
 y'_{10} &= y_{11} \\
 y'_{11} &= Lb \left[f\chi' - \frac{1}{2} f'\chi + S \left(2\chi + \frac{1}{2} \eta \chi' \right) \right] - Pe \left[\phi''(\chi + \delta) + \chi'\phi' \right]
 \end{aligned}$$

along with the boundary conditions:

$$\begin{aligned}
 f(0) = 0, f'(0) = \Delta_u f''(0), -\Delta_u g'(0) + g(0) = 1, \theta(0) = 1, \phi(0) = 1, \chi(0) = 1, \text{ at } \eta = 0, \\
 f'(\infty) \rightarrow 0, g(\infty) \rightarrow 0, \theta(\infty) \rightarrow 0, \phi(\infty) \rightarrow 0, \chi(\infty) \rightarrow 0, \text{ as } \eta \rightarrow \infty.
 \end{aligned}$$

This system of first order differential equations is coded in Matlab script.

Results and discussion

The computations are continued for suitable ranges of the influential parameters; $0.5 \leq M \leq 2.5, 0.1 \leq \beta \leq 2.5, 0.1 \leq m \leq 0.5, 0.1 \leq \lambda \leq 0.5, 0.5 \leq Nr \leq 2.5, 0.5 \leq Rb \leq 2.5, 0.1 \leq \Delta_u \leq 0.5, 1.0 \leq Br \leq 3.0, 0.1 \leq Nb \leq 0.5, 0.01 \leq Nt \leq 0.05, 6.0 \leq Pr \leq 8.0, 0.1 \leq Rd \leq 0.5, 1.0 \leq Sc \leq 5.0, 1.0 \leq Lb \leq 5.0, 1.0 \leq Pe \leq 5.0, 1.0 \leq \Omega \leq 5.0$. The fixed values for the parameters are chosen arbitrarily $M = 2.0, \beta = 0.5, m = 1.0, \lambda = 0.1, Nr = 0.1, Rb = 0.1, \Delta_u = 1.0, Br = 1.0, Nb = 0.1, Nt = 0.1, Pr = 7.0, Rd = 0.1, Sc = 4.0, Lb = 1.0, Pe = 1.0$ and $\Omega = 0.3$. Tables 1 and 2 show the comparison of the current numerical study with already published research work (Chamka et al.³⁵ and Deebani et al.³⁶). There seems a good correlation among the results. Thus numerical approach is validated and the computational procedure is continued.

It is to mention that throughout the graphs, green solid lines represent the steady case while red dotted lines represent unsteady case. Figure 2a shows the behavior of magnetic parameter *M* on velocity profile. It is seen that velocity decreases when *M* takes larger values. From the figure, it is seen that velocity decreases more rapidly for unsteady case than that of steady case. Physically, the basic reason behind this retardation is the Lorentz force produces resistance to the motion of fluid. Due to this resistance, velocity decreases. Figure 2b shows the effect

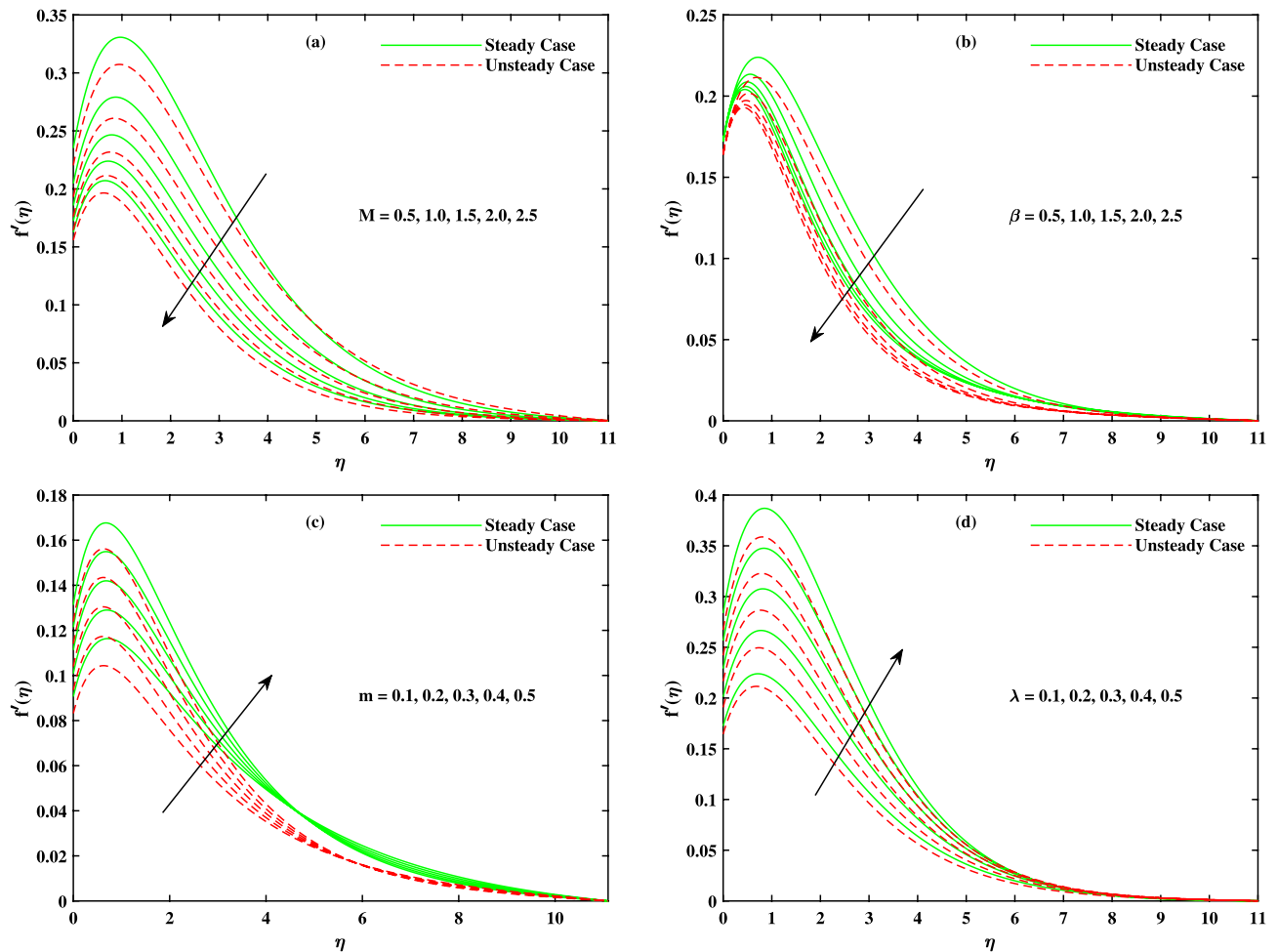


Figure 2. Fluctuation in x-direction velocity $f'(\eta)$ with (a) M , (b) β , (c) m and (d) λ .

of β on velocity profile. Decreasing behavior is observed in velocity profile when the value of β increases. The Williamson fluid parameter β is directly related to Γ , the time relaxation variable and hence retardation of flow is resulted. Opposite behavior for m is seen in Fig. 2c. Figure 2d shows the behavior of mixed convection parameter λ on velocity profile. It is clearly seen that for both cases steady and unsteady, velocity increases when λ increases. This incremented mixed convection causes, the faster flow due to buoyancy forces. The basic phenomenon of this increment in the velocity profile is that when λ takes larger values, velocity of the fluid is enhanced. Figure 3a,b,c show the decreasing behavior in velocity profile when buoyancy ratio parameter Nr , Rayleigh number Rb and Δ_u increase respectively. The basic phenomenon of this retardation in velocity profile is that there occurs more resistance in horizontal direction of fluid flow with larger values of these parameters. The effect of M , β , m and Δ_u on velocity $g(\eta)$ is observed in Fig. 4. It is clear from the figure that velocity decreases when values of above said non-dimensional parameters increase. Figure 5 shows the impact of M , Br , Nb , Nt , Pr and Rd on temperature profile. It is observed from Fig. 5a,b that temperature increases with the rising values of M and Br . As mentioned earlier, the fluid velocity decreases against m , the kinetic energy is converted in heat energy and hence temperature of fluid is risen. Physically, Brinkman number increase the thermal field of the fluid flow for higher estimations. Due to this, a smaller amount of thermal conduction to the fluid occur. Figure 5c,d show the behavior of Nb and Nt on temperature profile. From the figure, it is seen that temperature rises with the rising values of Nb and Nt . The basic concept for increase in temperature due to Brownian motion is that the nanoparticles are directly related with temperature, which means kinetic energy of these particles increases when temperature is enhanced. Also, for thermophoresis parameter, particles move from hotter surface to colder surface, thus temperature of fluid increases. Figure 5e shows the temperature decreases with rising values of Pr (Prandtl number). Physically Pr is inversely proportional to thermal diffusivity which causes reduction in temperature. Figure 5f shows the effect of radiation parameter Rd on temperature profile. It is noted that temperature increases with rising values of Rd . The basic reason behind is that a large amount of heat is produced in radiation process. Figure 6 shows the effect of Nb , Nt and Sc on concentration profile. For rising values of Nt , the concentration increases rapidly while it goes down for Nb and Sc . Figure 7 shows the effect of Lb , Pe and δ on motile density profile. It is clearly seen that the motile microorganisms profile goes down when the values of Lb , Pe and δ are uplifted. The basic reason behind this retardation of Pe is that the diffusivity of living microorganisms decreases down when Peclet number takes larger values. The effect of skin friction factor due to different parameters like M , β , m , λ , Nr , Rb and Δ_u for both steady and unsteady cases can be seen in Table 3. With the rising values of M , skin friction factor increases

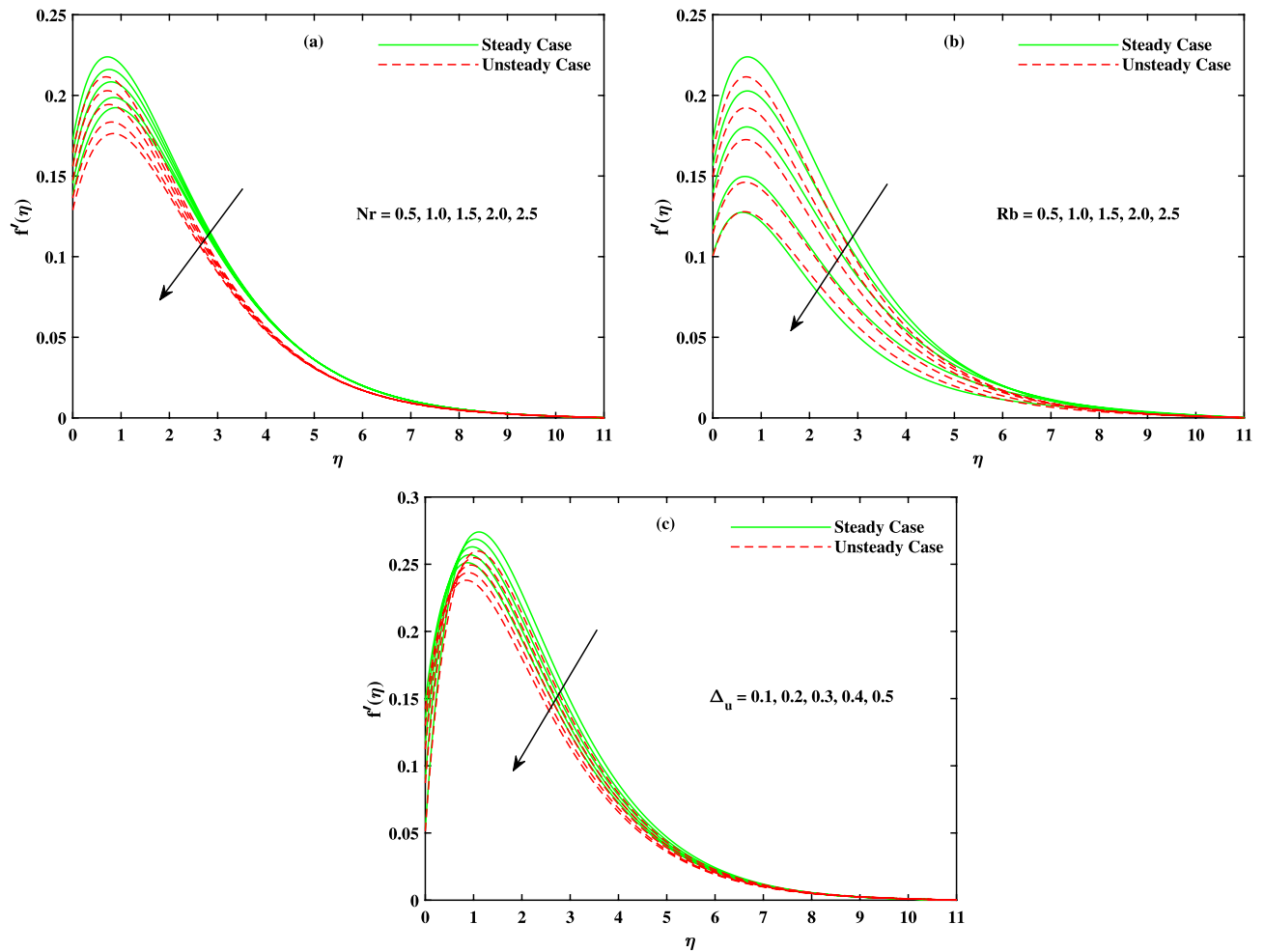


Figure 3. Fluctuation in x-direction velocity $f'(\eta)$ with (a) Nr , (b) Rb and (c) Δ_u .

more for steady case than that of unsteady case values. When β value increases, steady case decrease more than unsteady case. As m increases, steady case shows more gain in values than unsteady case. When λ increases, steady case values increase more than unsteady case values. However, an increase in Nr results in decrease in the values of steady case and unsteady case too, but there is more decrease in steady case. For increase in the values of Rb , there is an equal amount of decrease in values for both cases. For Δ_u values, both case values increase equally as Δ_u increases. Table 4 shows the results of $g'(0)$ for M , β , m and Δ_u for both steady and unsteady cases. It is clearly seen that as M increases, the values of steady case increase more than the values of unsteady case. On the other hand, increase in the values of β , m and Δ_u causes more decrease in the values of steady case than that of unsteady case. Table 5 displays the results for $\theta'(0)$ when Rd , Nb , Nt and Br are in action for both cases. It is seen that Rd increases more for unsteady case than that of steady case. Contrary the values of Nb , Nt and Br decrease more for unsteady cases than steady cases. In Table 6, the effect of Sherwood number for different parameters Sc , Nb , Nt and Γ are shown. As the values of Sc and Nb increase, Sherwood number increase. As Nt value increase, there occur more increase for unsteady case than steady case. For Γ values, there is more increase in steady case than unsteady case as Γ increases. Table 7 shows Lb , Pe and δ results for $\chi'(0)$. As Lb , Pe and δ values increase, there is more increase in the values for unsteady cases than that for steady cases.

Conclusions

Numerical application is made for magnetohydrodynamic flow of Williamson nanofluid transport across a rotating cone. Bioconvection of microorganisms and radiative heat transfer mode are incorporated. The salient findings are summarized as below:

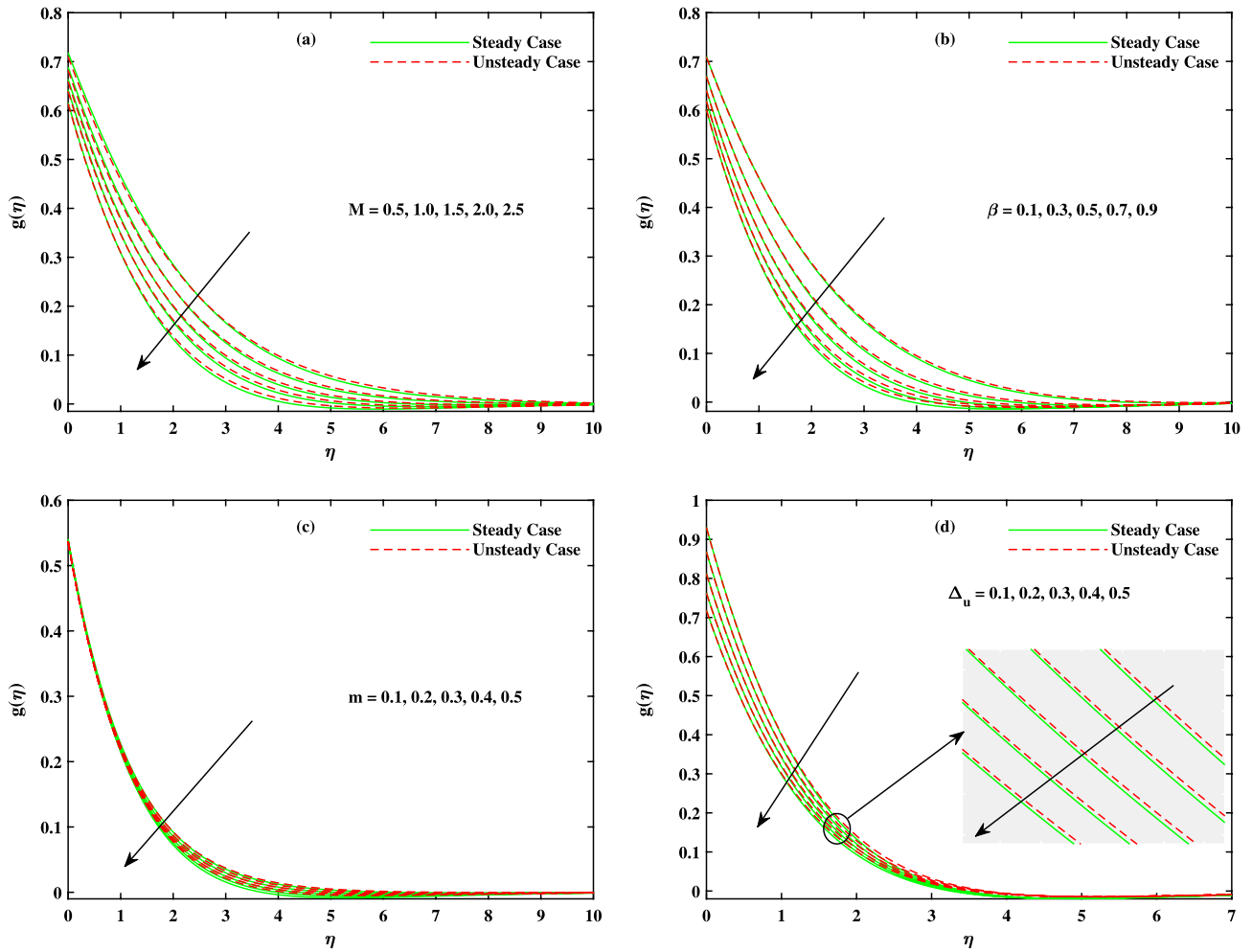


Figure 4. Fluctuation in y-direction velocity $g(\eta)$ with (a) M , (b) β , (c) m and (d) Δ_u .

- It is observed that velocity $f'(\eta)$ decreases when M , β , Nr , Rb , and Δ_u uplifts. Opposite behavior is seen for m and λ .
- it can also be seen that velocity $g'(\eta)$ decreases when M , β , m and Δ_u take larger values.
- When M , Br , Nb , Nt and Rd takes larger values temperature profile $\theta'(\eta)$ decreases. While $\theta'(\eta)$ increases when Pr uplifts.
- It is seen clearly seen that concentration profile $\phi'(\eta)$ decreases when Nb , Sc , Γ take larger values. Concentration profile $\phi'(\eta)$ increases when Nt uplift.
- Motile density profile $\chi'(\eta)$ decreases when Lb , Pe and Ω take larger values.
- Skin friction factor $f''(0)$ increases when M , m and λ take larger values While decreases when β , Nr , Rb and Δ_u uplifted.
- Skin friction factor $g'(0)$ increases when M take larger value while decreases for β , m and Δ_u .
- Nusselt number $\theta'(0)$ decreases when Nb , Nt and Br take larger values but rises when Rd upsurge.
- Sherwood number $\phi'(0)$ increases when Sc , Nb and Nt uplifted.
- Motile density number $\chi'(0)$ increases when Lb , Pe and δ take larger values.

Future work

This work can be further studied for hybrid nanofluid flow across stretching and rotating cone.

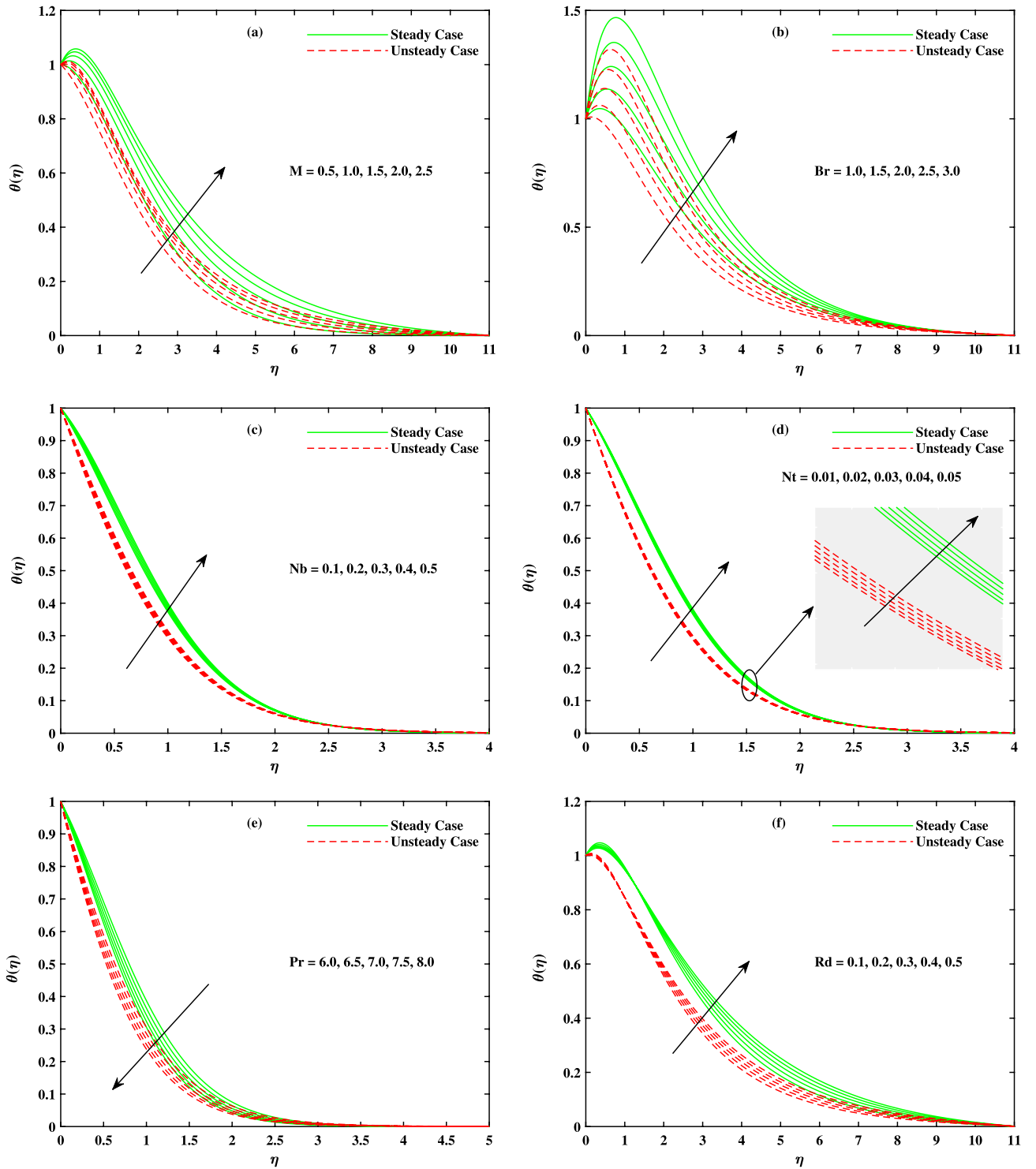


Figure 5. Fluctuation in temperature $\theta(\eta)$ with (a) M , (b) Br , (c) Nb , (d) Nt , (e) Pr and (f) Rd .

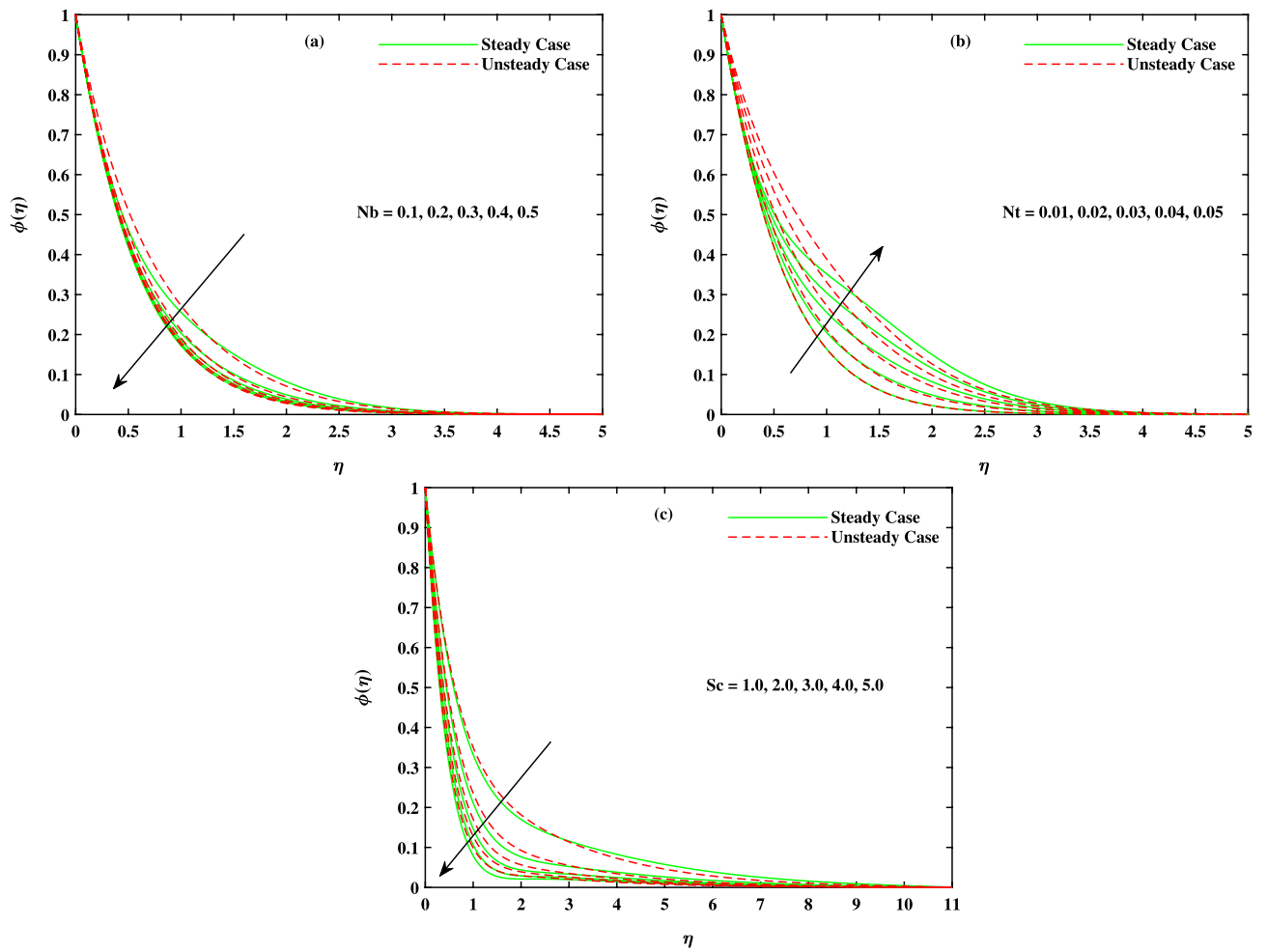


Figure 6. Fluctuation in concentration $\phi(\eta)$ with (a) Nb , (b) Nt and (c) Sc .

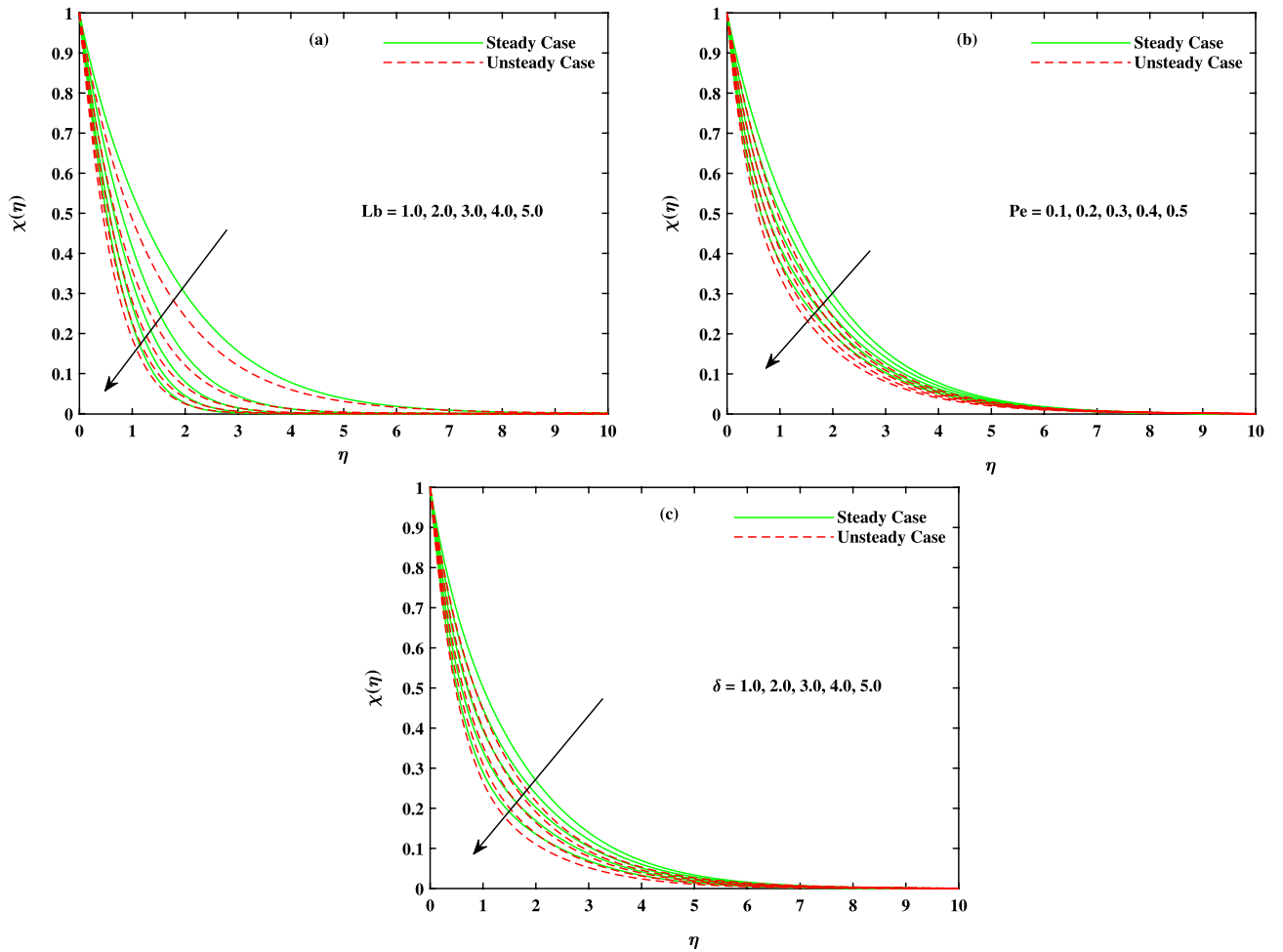


Figure 7. Fluctuation in motile density $\chi(\eta)$ with (a) Lb , (b) Pe and (c) δ .

M	β	m	λ	Nr	Rb	Δ_u	Steady Case	Unsteady Case
1.0	0.5	1.0	0.1	0.1	0.1	1.0	0.3660	0.3254
1.5							0.4156	0.4007
2.0							0.4724	0.4511
2.0	0.5						0.4724	0.4511
	1.0						0.3178	0.3026
	1.5						0.2648	0.2516
	0.5	0.5					0.3500	0.3308
		1.0					0.4724	0.4511
		1.5					0.5542	0.5297
		1.0	0.1				0.4724	0.4511
			0.2				0.5152	0.4889
			0.3				0.5556	0.5251
			0.1	0.1			0.4724	0.4511
				0.3			0.4636	0.4419
				0.5			0.4549	0.4326
				0.1	0.1		0.4724	0.4724
					0.3		0.4584	0.4584
					0.5		0.4443	0.4443
					0.1	0.1	1.4834	1.4834
						0.5	0.8209	0.8209
						1.0	0.4724	0.4724

Table 3. Results of skin friction factor $-f''(0)$ in x-direction for various parameters.

M	β	m	Δ_u	Steady Case	Unsteady Case
1.0	0.5	1.0	1.0	1.1121	1.1260
1.5				1.2176	1.2279
2.0				1.3022	1.3100
2.0	0.5			1.3022	1.3100
	1.0			0.9735	0.9779
	1.5			0.8130	0.8546
	0.5	0.5		1.3612	1.3695
		1.0		1.3022	1.3100
		1.5		1.2349	1.2429
		1.0	0.1	2.0165	2.0468
			0.5	1.6381	1.6536
			1.0	1.3022	1.3100

Table 4. Results of skin friction factor $g'(0)$ in y-direction for various parameters.

Rd	Nb	Nt	Br	Steady Case	Unsteady Case
0.1	0.1	0.1	1.0	0.5787	1.0386
0.2				0.6186	1.0946
0.3				0.6571	1.1485
0.1	0.1			0.5787	1.0386
	0.2			0.5392	0.9919
	0.3			0.5013	0.9469
	0.1	0.01		0.6031	1.0656
		0.05		0.5922	1.0535
		0.1		0.5787	1.0386
		0.1	0.1	1.0168	1.4133
			0.5	0.8219	1.2468
			1.0	0.5787	1.0386

Table 5. Results of Nusselt number $-\theta'(0)$ for various parameters.

Sc	Nb	Nt	Steady Case	Unsteady Case
4.0	0.1	0.1	1.6753	1.4135
5.0			1.8858	1.6290
6.0			2.0729	1.8215
4.0	0.1		1.6753	1.4135
	0.2		1.6796	1.5722
	0.3		1.6807	1.6248
	0.1	0.01	1.6568	1.6667
		0.05	1.6620	1.5503
		0.1	1.6753	1.4135

Table 6. Results of Sherwood number $-\phi'(0)$ for various parameters.

Lb	Pe	δ	Steady Case	Unsteady Case
0.1	0.1	0.1	0.3011	0.3188
0.5			0.4357	0.5327
1.0			0.5721	0.7064
1.0	0.1		0.5721	0.7064
	0.2		0.7326	0.8310
	0.3		0.8945	0.9572
	0.1	0.1	0.5721	0.7064
		0.2	0.5862	0.7167
		0.3	0.6002	0.7271

Table 7. Results of motile density number $-\chi'(0)$ for various parameters.

Data availability

The datasets used during the current study available from the corresponding author on reasonable request.

Received: 24 September 2022; Accepted: 26 December 2022

Published online: 31 December 2022

References

- Choi, S. U. & Eastman, J. A. Enhancing thermal conductivity of fluids with nanoparticles. *Tech. rep., Argonne National Lab. (ANL), Argonne, IL (United States)* (1995).
- Abbas, S. Z. *et al.* Modeling and analysis of unsteady second-grade nanofluid flow subject to mixed convection and thermal radiation. *Soft Comput.* **26**(3), 1033–1042 (2022).
- Wang, F. *et al.* The effects of nanoparticle aggregation and radiation on the flow of nanofluid between the gap of a disk and cone. *Case Stud. Therm. Eng.* **33**, 101930 (2022).
- Punith Gowda, R., Baskonus, H. M., Naveen Kumar, R., Prasannakumara, B. & Prakasha, D. Computational investigation of Stefan blowing effect on flow of second-grade fluid over a curved stretching sheet. *Int. J. Appl. Comput. Math.* **7**(3), 1–16 (2021).
- Naveen Kumar, R., Gowda, R., Gireesha, B. & Prasannakumara, B. Non-Newtonian hybrid nanofluid flow over vertically upward/downward moving rotating disk in a Darcy–Forchheimer porous medium. *Eur. Phys. J. Spec. Top.* **230**(5), 1227–1237 (2021).
- Gowda, R. P. *et al.* Thermophoretic particle deposition in time-dependent flow of hybrid nanofluid over rotating and vertically upward/downward moving disk. *Surf. Interfaces* **22**, 100864 (2021).
- Jyothi, A., Kumar, R. N., Gowda, R. P. & Prasannakumara, B. Significance of Stefan blowing effect on flow and heat transfer of Casson nanofluid over a moving thin needle. *Commun. Theor. Phys.* **73**(9), 095005 (2021).
- Li, Y.-X. *et al.* Dynamics of aluminum oxide and copper hybrid nanofluid in nonlinear mixed Marangoni convective flow with entropy generation: Applications to renewable energy. *Chin. J. Phys.* **73**, 275–287 (2021).
- Yusuf, T. A., Mabood, F., Prasannakumara, B. & Sarris, I. E. Magneto-bioconvection flow of Williamson nanofluid over an inclined plate with gyrotactic microorganisms and entropy generation. *Fluids* **6**(3), 109 (2021).
- Prasannakumara, B. Numerical simulation of heat transport in Maxwell nanofluid flow over a stretching sheet considering magnetic dipole effect. *Part. Differ. Equ. Appl. Math.* **4**, 100064 (2021).
- Benos, L. T., Karvelas, E. & Sarris, I. A theoretical model for the magnetohydrodynamic natural convection of a CNT-water nanofluid incorporating a renovated Hamilton–Crosser model. *Int. J. Heat Mass Transf.* **135**, 548–560 (2019).
- Sarris, I., Kassinos, S. C. & Carati, D. Large-eddy simulations of the turbulent Hartmann flow close to the transitional regime. *Phys. Fluids* **19**(8), 085109 (2007).
- Sarris, I., Tsiakaras, P., Song, S. & Vlachos, N. A three-dimensional CFD model of direct ethanol fuel cells: Anode flow bed analysis. *Solid State Ion.* **177**(19–25), 2133–2138 (2006).
- Karvelas, E., Liosis, C., Benos, L., Karakasidis, T. & Sarris, I. Micromixing efficiency of particles in heavy metal removal processes under various inlet conditions. *Water* **11**(6), 1135 (2019).
- Gowda, R. P., Kumar, R. N., Prasannakumara, B., Nagaraja, B. & Gireesha, B. Exploring magnetic dipole contribution on ferro-magnetic nanofluid flow over a stretching sheet: An application of Stefan blowing. *J. Mol. Liq.* **335**, 116215 (2021).
- Gowda, R. P. *et al.* Computational modelling of nanofluid flow over a curved stretching sheet using Koo–Kleinstreuer and Li (KKL) correlation and modified Fourier heat flux model. *Chaos Solitons Fractals* **145**, 110774 (2021).
- Punith Gowda, R. J., Naveen Kumar, R., Jyothi, A. M., Prasannakumara, B. C. & Sarris, I. E. Impact of binary chemical reaction and activation energy on heat and mass transfer of Marangoni driven boundary layer flow of a non-Newtonian nanofluid. *Processes* **9**(4), 702 (2021).
- Gowda, R., Kumar, R. N., Rauf, A., Prasannakumara, B. & Shehzad, S. Magnetized flow of Sutterby nanofluid through Cattaneo–Christov theory of heat diffusion and Stefan blowing condition. *Appl. Nanosci.* (2021). <https://doi.org/10.1007/s13204-021-01863-y>
- Gowda, R., Rauf, A., Naveen Kumar, R., Prasannakumara, B. & Shehzad, S. Slip flow of Casson–Maxwell nanofluid confined through stretchable disks. *Indian J. Phys.* **96**(7), 2041–2049 (2022).
- Williamson, R. V. The flow of pseudoplastic materials. *Ind. Eng. Chem.* **21**(11), 1108–1111 (1929).
- Srinivas Reddy, C., Ali, F., Mahanthesh, B. & Naikoti, K. Irreversibility analysis of radiative heat transport of Williamson material over a lubricated surface with viscous heating and internal heat source. *Heat Transf.* **51**(1), 395–412 (2022).
- Abdal, S., Siddique, I., Alrowaili, D., Al-Mdallal, Q. & Hussain, S. Exploring the magnetohydrodynamic stretched flow of Williamson maxwell nanofluid through porous matrix over a permeated sheet with bioconvection and activation energy. *Sci. Rep.* **12**(1), 1–12 (2022).
- Qayyum, S. *et al.* Interpretation of entropy generation in Williamson fluid flow with nonlinear thermal radiation and first-order velocity slip. *Math. Methods Appl. Sci.* **44**(9), 7756–7765 (2021).
- Waqas, M. *et al.* Interaction of heat generation in nonlinear mixed/forced convective flow of Williamson fluid flow subject to generalized Fourier's and Fick's concept. *J. Mater. Res. Technol.* **9**(5), 11080–11086 (2020).
- Chu, Y.-M., Nazir, U., Sohail, M., Selim, M. M. & Lee, J.-R. Enhancement in thermal energy and solute particles using hybrid nanoparticles by engaging activation energy and chemical reaction over a parabolic surface via finite element approach. *Fractal Fract.* **5**(3), 119 (2021).

26. Chu, Y.-M. *et al.* Combined impacts of heat source/sink, radiative heat flux, temperature dependent thermal conductivity on forced convective Rabinowitsch fluid. *Int. Commun. Heat Mass Transf.* **120**, 105011 (2021).
27. Abdal, S. *et al.* Significance of magnetohydrodynamic Williamson Sutterby nanofluid due to a rotating cone with bioconvection and anisotropic slip. *ZAMM J. Appl. Math. Mech./Z. Angew. Math. Mech.* <https://doi.org/10.1002/zamm.202100503> (2022).
28. Habib, U., Abdal, S., Siddique, I. & Ali, R. A comparative study on micropolar, Williamson, maxwell nanofluids flow due to a stretching surface in the presence of bioconvection, double diffusion and activation energy. *Int. Commun. Heat Mass Transf.* **127**, 105551 (2021).
29. Yahya, A. U. *et al.* Implication of bio-convection and Cattaneo–Christov heat flux on Williamson Sutterby nanofluid transportation caused by a stretching surface with convective boundary. *Chin. J. Phys.* **73**, 706–718 (2021).
30. Ramesh, K. *et al.* Bioconvection assessment in Maxwell nanofluid configured by a Riga surface with nonlinear thermal radiation and activation energy. *Surf. Interfaces* **21**, 100749 (2020).
31. Song, Y.-Q. *et al.* Applications of modified Darcy law and nonlinear thermal radiation in bioconvection flow of micropolar nanofluid over an off centered rotating disk. *Alex. Eng. J.* **60**(5), 4607–4618 (2021).
32. Farooq, U. *et al.* Thermally radioactive bioconvection flow of Carreau nanofluid with modified Cattaneo–Christov expressions and exponential space-based heat source. *Alex. Eng. J.* **60**(3), 3073–3086 (2021).
33. Song, Y.-Q. *et al.* Bioconvection analysis for Sutterby nanofluid over an axially stretched cylinder with melting heat transfer and variable thermal features: A Marangoni and Solutal model. *Alex. Eng. J.* **60**(5), 4663–4675 (2021).
34. Chu, Y.-M. *et al.* Combined impact of Cattaneo–Christov double diffusion and radiative heat flux on bio-convective flow of maxwell liquid configured by a stretched nano-material surface. *Appl. Math. Comput.* **419**, 126883 (2022).
35. Chamkha, A. J. & Al-Mudhaf, A. Unsteady heat and mass transfer from a rotating vertical cone with a magnetic field and heat generation or absorption effects. *Int. J. Therm. Sci.* **44**(3), 267–276 (2005).
36. Deebani, W., Tassaddiq, A., Shah, Z., Dawar, A. & Ali, F. Hall effect on radiative Casson fluid flow with chemical reaction on a rotating cone through entropy optimization. *Entropy* **22**(4), 480 (2020).
37. Faiz, M. *et al.* Multiple slip effects on time dependent axisymmetric flow of magnetized Carreau nanofluid and motile microorganisms. *Sci. Rep.* **12**(1), 1–14 (2022).
38. Ali, L., Siddique, I., Salamat, N., Hussain, S. & Abdal, S. The significance of magnetohydrodynamics Sutterby nanofluid flow with concentration depending properties across stretching/shrinking sheet and porosity. *Int. J. Mod. Phys. B* **36**, 2250223 (2022).
39. Abdal, S. *et al.* On time-dependent rheology of Sutterby nanofluid transport across a rotating cone with anisotropic slip constraints and bioconvection. *Nanomaterials* **12**(17), 2902 (2022).
40. Ali, L., Abdal, S., Hussain, S., Salamat, N. & Mariam, A. Numerical analysis of concentration-dependent physical properties and bioconvection for Williamson nanofluid flow due to stretching/shrinking sheet. *Int. J. Mod. Phys. B* <https://doi.org/10.1142/S0217979223500662> (2022).
41. Siddique, I., Habib, U., Ali, R., Abdal, S. & Salamat, N. Bioconvection attribution for effective thermal transportation of upper convected Maxwell nanofluid flow due to an extending cylindrical surface. *Int. Commun. Heat Mass Transf.* **137**, 106239 (2022).
42. Ali, L., Wu, Y.-J., Ali, B., Abdal, S. & Hussain, S. The crucial features of aggregation in TiO_2 -water nanofluid aligned of chemically comprising microorganisms: A FEM approach. *Comput. Math. Appl.* **123**, 241–251 (2022).
43. Abdal, S., Siddique, I., Din, I. S. U. & Hussain, S. On prescribed thermal distributions of bioconvection Williamson nanofluid transportation due to an extending sheet with non-Fourier flux and radiation. *Waves Random Complex Media.* (2022). <https://doi.org/10.1080/17455030.2022.2136416>
44. Din, I. S. U. *et al.* On heat and flow characteristics of Carreau nanofluid and tangent hyperbolic nanofluid across a wedge with slip effects and bioconvection. *Case Stud. Therm. Eng.* **39**, 102390 (2022).
45. Abdal, S., Siddique, I., Salamat, N. & Ud Din, I. S. Nano-bio-film flow of Williamson fluid due to a non-linearly extending/contracting surface with non-uniform physical properties. *Waves Random Complex Media.* (2022). <https://doi.org/10.1080/17455030.2022.2146233>.

Acknowledgements

This work was partially funded by the research center of the Future University in Egypt, 2022.

Author contributions

Conceptualization; S.A. and I.S. Methodology; M.B. and S.H. Investigation; I.S. and S.M.E. Funding acquisition; S.M.E. Writing-original draft preparation; S.A. and M.B. Validation; S.H. and S.M.E. Writing-review and editing; I.S. and S.M.E.. Supervision; S.H. and I.S. All authors have read and agreed to the published version of the manuscript.

Competing interests

The authors declare no competing interests.

Additional information

Correspondence and requests for materials should be addressed to I.S.

Reprints and permissions information is available at www.nature.com/reprints.

Publisher's note Springer Nature remains neutral with regard to jurisdictional claims in published maps and institutional affiliations.



Open Access This article is licensed under a Creative Commons Attribution 4.0 International License, which permits use, sharing, adaptation, distribution and reproduction in any medium or format, as long as you give appropriate credit to the original author(s) and the source, provide a link to the Creative Commons licence, and indicate if changes were made. The images or other third party material in this article are included in the article's Creative Commons licence, unless indicated otherwise in a credit line to the material. If material is not included in the article's Creative Commons licence and your intended use is not permitted by statutory regulation or exceeds the permitted use, you will need to obtain permission directly from the copyright holder. To view a copy of this licence, visit <http://creativecommons.org/licenses/by/4.0/>.

© The Author(s) 2022